Chapter 5

Adaptive configuration selection method

Having studied the estimator's behavior for several different configurations and conditions, there is still uncertainty about the best performance it can achieve. In the considered system, the hydrophone configuration has a decisive role on the achieved precision, as demonstrated. Therefore, a way to optimize the system's estimation would be to choose, for each position of the acoustic source, the configuration that returns the best estimation and thus the one that should be employed.

In a field scenario where a vehicle is searching for an acoustic transmitter, as it is navigating and readjusting its trajectory, the relative direction that is being estimated in real time is changing. Therefore, the system's performance can vary and arises the necessity of having different angles of vision from the hydrophones to the target. To resolve this issue, the proposed method assumes that the used USBL system integrates more than four hydrophones placed in known positions. This way, it is possible to dynamically reconfigure which four hydrophones are used at a time leading to an estimation that is optimal for the available sensors.

Another possibility is to determine through the same techniques which configuration of four hydrophones, tested in various positions along the vehicle, is the overall best for short and long range estimation. This can lead to a moderate compromise of the estimate accuracy, however decreases the number sensors that are employed and therefore the cost of the system.

This chapter is dedicated to explaining the methodological approach, the main findings and conclusions that were driven from the formulated optimal reconfiguration method. Firstly, the developed Monte Carlo method is explained, including the theoretical details as well as the developed algorithm. Thereafter, its functional demonstration through simulation is presented, followed by a brief comparison with the results obtained by the Crámer-Rao bound method previously implemented. Lastly, the implementation of the optimal solution based on range is presented and a practical comparison is established with the alternative FIM mechanism.

5.1 Monte Carlo Approach

The developed algorithm serves as a tool to determine which is the best available hydrophone configuration for a certain target position. This approach uses a Monte Carlo method which is useful to solve problems that are deterministic in nature through repetition and application of random parameters. Additionally, it makes use of the developed estimator, which is comprehensively explained in 4.2.2, to estimate the target position for each sensor configuration.

For this experiment, it is considered a total of nine hydrophones, whose positions are contained in $matrix_{r_i}$, defined by table 5.1. Each column expresses the coordinates of each hydrophone, r_i, where the value of x_i is in the first row, the value of y_i in the second row and the value of z_i in the third row. Additionally, it is assumed $q = 0.1$, $w = 0.1$ and $e = \frac{\sqrt{2}}{2} * w$.

	r1	r2	r3	r4	r5	r6	r7	r8	r9
x	q	0	0	0	0	0	0	0	0
y	0	0	0	w	-w	e	e	-e	-e
z	0	w	-w	0	0	e	-e	e	-e

Table 5.1: Position coordinates for the implementation using 9 hydrophones

These positions are arranged so that they can mimic a possible deployment in an AUV, as represented in figure 5.1, where hydrophone r_1 is placed in front of the vehicle and hydrophones r_2 to r_9 form a circle with a 10cm radius around the vehicle.
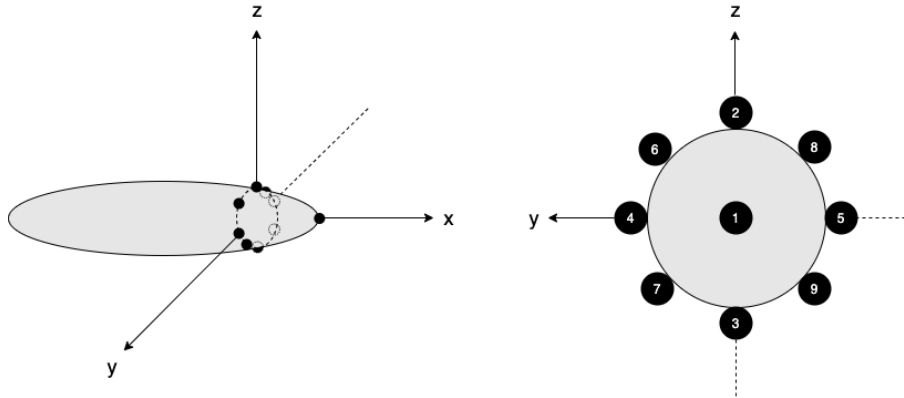

Figure 5.1: Hydrophone positions for the implementation using 9 hydrophones

Since the used configuration has to be three dimensional, it is defined that hydrophone r_1 always integrates the configuration as it is the only one that covers a third dimension. Accordingly, the number of possibilities is combinations of three out of eight, $C(8,3)$, making up a total of 56 combinations. Each of these configurations are associated with a number from 1 to 56 and the hydrophones that integrate each of them are outlined in table A.1 for consultation when necessary.

Having the system presented, the algorithm will be explained next. For the sake of clarity, the algorithm was outlined in pseudo code and separated into two main parts, where 1 is integrated in 2.

Algorithm 1 Determines the average azimuth errors, elevation errors and MSE for a set of hydrophone configurations

---

1: **for** `all k configurations` **do**
2:    **for** `all i estimation repetition` **do**
3:       $estimator(s, config(k), error)$ {returns estimate in Cartesian and spherical coordinates}
4:       `accum_estimate(i)` $\leftarrow$ `result of the estimator in each repetition`
5:       `accum_error_azimuth(i)` $\leftarrow$ `azimuth error in each repetition`
6:       `accum_error_elevation(i)` $\leftarrow$ `elevation error in each repetition`
7:    **end for**
8:    $mean\_estimate \leftarrow \dfrac{accum\_estimate}{accum\_samples}$
9:
10:    $deviation\_azimuth(config) = std(accum\_error\_azimuth);$
11:    $deviation\_elevation(config) = std(accum\_error\_elevation);$
12:    $error\_azimuth(config) = mean(accum\_error\_azimuth);$
13:    $error\_elevation(config) = mean(accum\_error\_elevation);$
14:
15:    $mse(config) = \sqrt{error\_azimuth(config)^2 + error\_elevation(config)^2};$
16: **end for**

Algorithm 1 is dedicated to computing the average azimuth error, elevation error and MSE for each of the $k = 56$ hydrophone configuration, in order to understand which of them achieves the minimum deviations when estimating a specific position. In order to do so, for each possible hydrophone configuration, the chosen acoustic source position s was estimated $i = 1000$ times (line 3), using the developed estimator. This includes an injected error to the TDoA that follows a Gaussian distribution with zero mean and a configurable variance of σ^2, i.e., $e_i \sim \mathcal{N}(0, \sigma^2)$. The result of this repetition would be an estimate cloud around the absolute s position, which indicates the estimation variation achieved by a certain configuration for a specific position in space. At each stage of the repetition, the estimate is accumulated and the errors of azimuth and elevation are calculated, similarly to the process described in the accuracy analysis **??** of the estimator. Therefore, after computing all estimation repetitions, it is possible to extract four essential parameters that define the quality of the estimation for each configuration: a mean estimate (line 8); the azimuth and elevation standard deviations (lines 10 and 11); the azimuth and elevation estimation errors (lines 12 and 13); the MSE (line 15).

Finally, using the obtained parameters it is possible to determine three configurations that lead to the best estimation regarding MSE, azimuth deviation and elevation deviation. However, there are two main issues that this simple algorithm does not take into account:

1. For the considered system conditions, the error that is introduced is sufficient to originate different results every time a position s is tested with the same injected error.

2. Assuming that the hydrophone system is deployed in an AUV, it is expected that every hydrophone has a blind spot, where the acoustic source can be located. Even though the

transmitted signals could still be received by these hydrophones, they would be distorted and could lead to misinformation so they should not be considered. Consequently the hydrophones that do not have line of sight to the transmitter should be disregarded as well.

In order to resolve both these problems, a second part of logic was developed, which is translated in pseudo code 2.

In order to turn this mechanism more robust and solve the first issue, it is considered that the experiment of algorithm 1 has to be reiterated a defined number of times to obtain coherent and conclusive answers. Having said this, algorithm 2 begins with a loop that reiterates $j = 10$ times the logic previously explained. Addressing the second issue, the *line_of_sight* function (line 7) is called, serving as filter to determine which hydrophones have line of sight to the estimated position. The mathematical definitions and conditions included in this function as well as the inputs and outputs are better clarified in the next subsection 5.1.1. Thereafter, all configurations that have full line of sight to the transmitter are extracted. Meanwhile, the azimuth deviations, elevation deviations and MSE are accumulated in each experiment reiteration (line 8 to 10) so that it is possible to obtain the definitive mean of these parameters for each configuration (line 12 to 14).

Algorithm 2 Determines the overall best configuration for a specific position estimation considering:
- multiple full experiments (Algorithm 1);
- only hydrophones with line of sight to the target.

1: **for** all j experiment reiterations **do**
2:      `*************************`
3:      `*** INSERT ALGORITHM 1 ***`
4:      `*************************`
5:
6:      $line\_of\_sight(mean\_estimate, matrix_{r_i})$ {returns which hydrophones have line of sight to the target}
7:
8:      $reit\_mse = reit\_mse + mse$
9:      $reit\_dev\_azimuth = reit\_error\_azimuth + deviation\_azimuth$
10:      $reit\_dev\_elevation = reit\_error\_elevation + deviation\_elevation$
11: **end for**
12: $mean\_MSE = reit\_mse \div j$
13: $mean\_dev\_azimuth = reit\_dev\_azimuth \div j$
14: $mean\_dev\_elevation = reit\_dev\_elevation \div j$
15:
16: `Extract the configurations that contain only hydrophones with line of sight`
17: `Form matrix with errors of only the configurations with full line of slight`
18:
19: $[best\_config\_for\_mse, \; overall\_min\_mse] = min(overall\_mse)$
20: $[best\_config\_for\_azimuth, \; overall\_min\_dev\_azimuth] = min(overall\_dev\_azimuth)$
21: $[best\_config\_for\_elevation, \; overall\_min\_dev\_elevation] = min(overall\_dev\_elevation)$

At this stage, it is possible to know already which are the configurations that are considered to achieve the minimum errors in each *j* reiteration and how many times each of them are chosen. However, these are still not filtered, thus they can contain hydrophones that have not line of sight

to the acoustic source. Consequently, the next step is to extract only the configuration with full LOS and form three matrices with the azimuth deviations, elevation deviations and MSE of these configurations. Having the final parameters calculated and filtered, the overall best configurations for each of the chosen parameters are given by the minimum of the matrices that contain said parameter (line 19 to 21), i.e. for all configurations with full LOS:

- The minimum obtained MSE corresponds to the configuration that more precisely estimates the position *s* in terms of MSE;

- The minimum obtained azimuth deviation corresponds to the configuration that more precisely estimates the position *s* in terms of azimuth;

- The minimum obtained elevation deviation corresponds to the configuration that more precisely estimates the position *s* in terms of elevation.

Additionally, it is possible to obtain the best configuration in terms of azimuth and elevation simultaneously, by computing the mean between the deviation of azimuth and elevation in each of the selected configurations. The minimum value obtained corresponds to the configuration which achieve the minimum the deviation in both parameters simultaneously.

5.1.1 Line of sight definition

As briefly explained before, when considering a set of hydrophones placed in the surface of an AUV, there will be blind regions for each of the hydrophones. Nonetheless, when an acoustic source is positioned in a blind region of an hydrophone, it still can receive a transmitted signal through reflections on path objects or reverberation in the AUV's surface. Since these signals would be distorted from the original, they could lead to misinformation after the processing if they were to be considered. For this reason, it is essential to exclusively consider configurations whose hydrophones have line of sight (LOS) to the transmitter.

In the present application, this feature is executed through function *line_of_sight* of algorithm 2, which outputs a vector containing all the hydrophones that have line of sight to the inputted transmitter position, *mean_estimate*, from the considered set $matrix_{r_i}$.

In order to define which hydrophones have LOS to a specific position in space, a region was defined for each hydrophone as its LOS region, ls_i. Thus, three simplifications were initially considered:

- The model for the vehicle is an approximation to a typical shape of an AUV using geometric shapes, as represented in 5.2, composed by a cylinder as the body with $2*w$ of diameter and a cone in the front with height equal to *q*;

- The regions for a $x \leq 0$ are defined as if the hydrophones were flat in the vehicle's surface, which leads to a simplified definition of the LOS region;
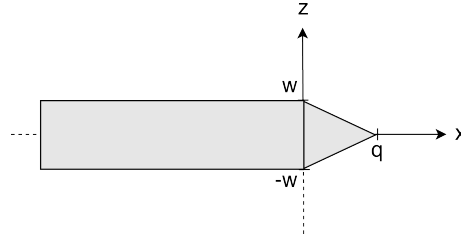
Figure 5.2: Model of AUV used to calculate the LOS region

- Since hydrophone r_1 is integrated in every configuration, there is no necessity of defining its LOS region.

Having these relations into account, the LOS regions are then defined separately for $x \leq 0$ and $x > 0$. When $x \leq 0$, the second simplification previously mentioned is applied so all ls_i are defined as the region greater/less or equal than the tangential to the position of hydrophone i in plane yz. These tangential equations are defined in 5.1 to 5.8.

$$ls_2 \leftarrow x \leq 0 \ \wedge \ z > r_{2_z} \tag{5.1}$$

$$ls_3 \leftarrow x \leq 0 \ \wedge \ z < r_{3_z} \tag{5.2}$$

$$ls_4 \leftarrow x \leq 0 \ \wedge \ y > r_{4_y} \tag{5.3}$$

$$ls_5 \leftarrow x \leq 0 \ \wedge \ y < r_{5_y} \tag{5.4}$$

$$ls_6 \leftarrow x \leq 0 \ \wedge \ z \geq -y + w\sqrt{2} \tag{5.5}$$

$$ls_7 \leftarrow x \leq 0 \ \wedge \ z \leq y - w\sqrt{2} \tag{5.6}$$

$$ls_8 \leftarrow x \leq 0 \ \wedge \ z \geq y + w\sqrt{2} \tag{5.7}$$

$$ls_9 \leftarrow x \leq 0 \ \wedge \ z \leq -y - w\sqrt{2} \tag{5.8}$$

By evaluating these equations, it is possible to infer that the LOS regions for $x \leq 0$ intersect each other, as illustrated in figure 5.3. The projection is correspondent to the yz plane with an inverted y-axis, in accordance with the previously presented model of the USBL system. Additionally, each colored line corresponds to the LOS region covered by the hydrophone with the same color. For instance, if a transmitter is located in $s_{cart}(-10, -10, -10)$, by analysis of the schematic it is observable that this position is covered by ls_3, ls_5 and ls_9, thus in line of sight of hydrophones 3,5 and 9.

Analogously, when $x > 0$, all ls_i are defined as the region greater/less or equal than the tangential to the position of hydrophone i in planes xz or xy, depending on the hydrophone's location. Dealing with the hydrophones positioned in the y and z-axis, r_2, r_3, r_4 and r_5, it is possible to directly formulate equations that help defining ls_2, ls_3, ls_4 and ls_5 since the tangent plane to these hydrophones is perpendicular to referential planes. However, when considering hydrophones r_6, r_7, r_8 and r_9, which are not positioned in any referential axis, the tangential plane which passes through the hydrophone and the front limit of the cone is not parallel to any of the
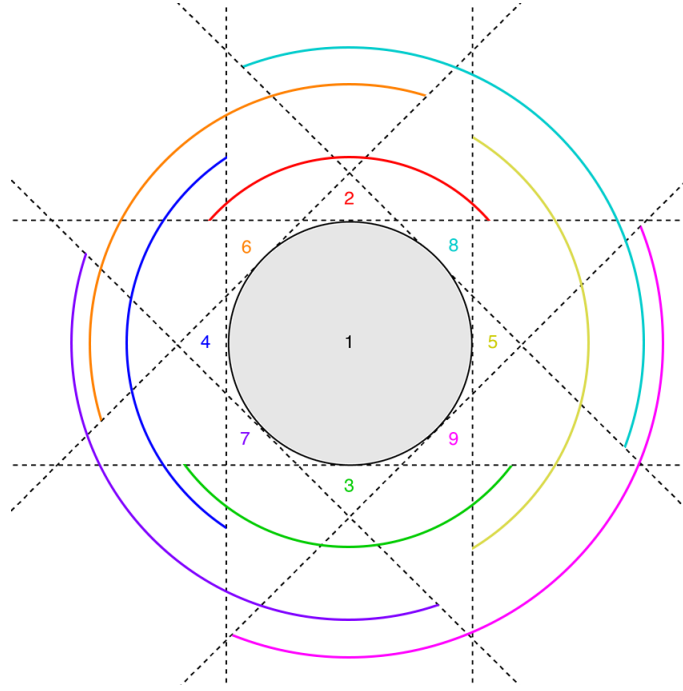
Figure 5.3: Line of sight regions in plane yz for x < 0

referential planes xy, xz or yz. Therefore, the equations that could define these planes require a rotation of the referential axis. In order to counter this issue, since the shape of the model projected in the yz plane is a circle , if hydrophones r_6, r_7, r_8 and r_9 are rotated a 45° angle around the x-axis, they can become coincident with the positions of r_2, r_4, r_5 and r_3 respectively. Additionally, when considering this rotation, the position of the transmitter would also be rotated the same angle to maintain their relative positions. Overall, the used equations are defined by relations 5.9 to 5.12, where the regarded x, y, z coordinates are the original transmitter position for ls_2, ls_3, ls_4, ls_5, and the rotated transmitter position for ls_6, ls_7, ls_8, ls_9.

$$ls_2, \ ls_6 \leftarrow x > 0 \ \wedge \ z \geq -\frac{w}{q}x + w \tag{5.9}$$

$$ls_3, \ ls_9 \leftarrow x > 0 \ \wedge \ z \leq \frac{w}{q}x - w \tag{5.10}$$

$$ls_4, \ ls_7 \leftarrow x > 0 \ \wedge \ y \geq -\frac{w}{q}x + w \tag{5.11}$$

$$ls_5, \ ls_8 \leftarrow x > 0 \ \wedge \ y \leq \frac{w}{q}x - w \tag{5.12}$$

After evaluating these equations and the limiting planes that they form, the projected regions of LOS for r_2, r_3, r_4 and r_5 are illustrated in 5.4, where their intersection is evident. The regions ls_2, ls_3, ls_4 and ls_5 are naturally similar to these, with an additional rotation of 45° around the x-axis.

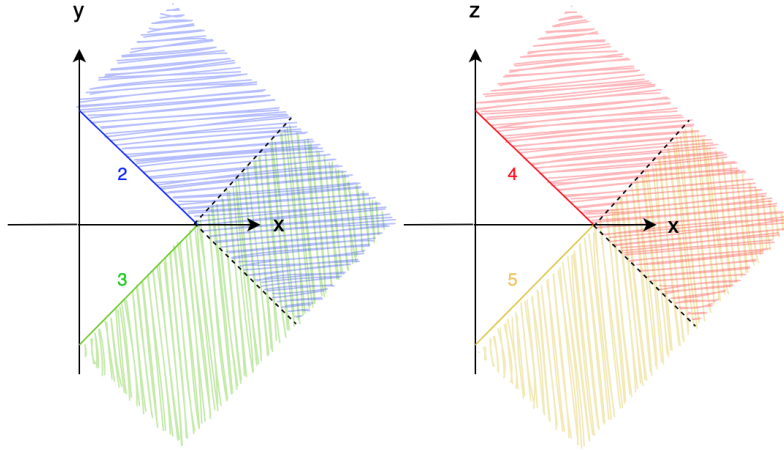In summary, it is possible to deduce that there is a larger quantity of different configurations

Figure 5.4: Line of sight regions in plane yx and zx for x ≥ 0

that cover the space for $x > 0$ than for $x \leq 0$ due to the model of the AUV and the considerations described in the course of this subsection. Therefore it is expected a better estimation for positions of the acoustic source with an azimuth angle between $-90°$ and $90°$.

5.2 Comprehensive study of geometric configurations performance

For the purpose of demonstrating the functionality of the implemented system, various acoustic source positions were tested and the results analyzed.

The first demonstration evaluates the achieved MSE, azimuth deviation and elevation deviation for $s_{cart}(10, 10, 10)$. After simulating, plot 5.5 demonstrate the results, where the obtained parametric errors are illustrated for each of the 56 formulated configurations. Additionally, the configurations which are marked with a red circle correspond to those whose hydrophones all have full line of sight to the transmitter and the green star indicates which is the configuration that achieves the lowest error. The results of this experiment are aggregated in table 5.2. For the present case, the hydrophones considered to have line of sight to the target are r_2, r_4, r_6, r_7 and r_8. The configuration with lowest MSE and azimuth deviation is number 8, composed by hydrophones r_1, r_2, r_4 and r_6, which are the directly closer to the target. The configuration that originates lowest elevation deviation is number 19, composed by r_1, r_2, r_7 and r_8, which maximizes the baseline of the sensors with line of sight.

Additionally, if the azimuth and elevation deviations are evaluated simultaneously, then the obtained plots can be overlaid to a clear comparison between results. Figure 5.6 represents this situation where, as the label indicates, the azimuth deviation in degrees is represented by the blue line, the pink line is the elevation deviation in degrees, the red and green circles represent the configurations with line of sight to the target and the green star indicates, once again, the configurations which achieve the minimum deviations in azimuth and elevation. Additionally, the cyan diamond reveals which of the configurations leads to the minimum mean between the
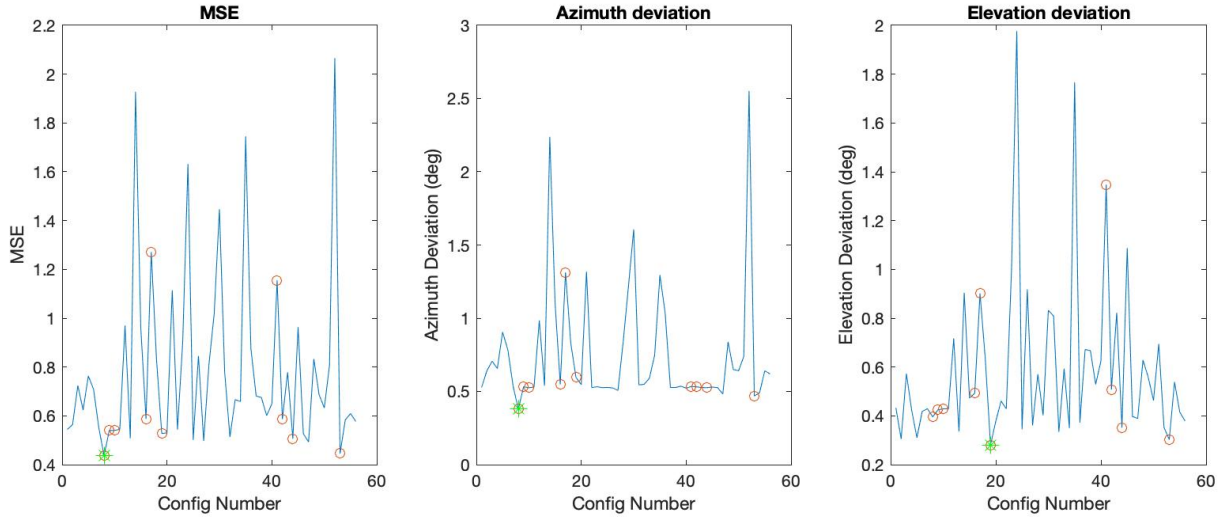
Figure 5.5: Errors obtained for all configurations when estimating
position $s_{cart}(10, 10, 10)$

azimuth and the elevation deviations. In this case, this corresponds to configuration number 53
which reaches a mean deviation of 0.385 degrees.

Figure 5.6: Overlaid azimuth and elevation deviations for all
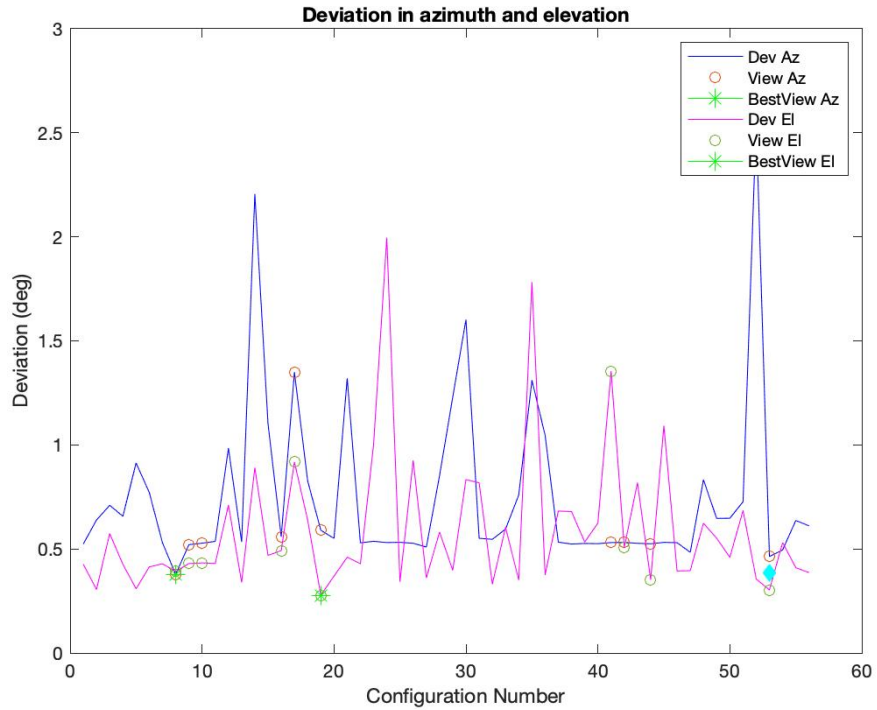configurations when estimating position $s_{cart}(10, 10, 10)$

In a second experiment, position $s_{cart}(100, 100, 100)$ is tested, which has the same azimuth and

elevation angles as the previous position and a norm 10 times larger. For this case, the error range of azimuth and elevation estimation is approximately the same and the norm estimation presents an error around 10 times larger. Additionally, as expected the configurations that lead to the lowest errors are the same as for the first experiment.

A set of tests were executed in order to compare the performance of various positions estimation and to extract behavior patterns for the chosen configurations. The collected data is present in table 5.2, where the position of the transmitter are given in Cartesian coordinates by (s_x, s_y, s_z) and for each of the performance parameters it is presented the obtained best configuration number and the minimum error achieved by it. It should also be noted that the notation $0_+/0_-$ indicates that for a theoretical position with a coordinate equal to zero it was returned a slightly positive/negative estimate of that same coordinate, due to the injected error.

s_{cart}			Azimuth		Elevation		Azimuth+Elevation		MSE	
x	y	z	Config	Min	Config	Min	Config	Min	Config	Min
10	10	10	8	0.377	19	0.278	53	0.385	8	0.434
-10	-10	-10	30	2.412	30	1.196	30	1.804	30	2.142
0_+	-10	-10	14	2.058	14	0.431	14	1.244	14	1.672
100	0_-	0_-	47	0.177	32	0.177	11	0.284	11	0.330
0_+	100	0_+	9	0.596	16	0.425	16	0.512	16	0.586
0_+	0_-	100	37	52.572	39	0.381	37	26.479	39	32.602
15	-10	5	48	0.364	3	0.218	27	0.346	27	0.399

Table 5.2: Summary of best configurations obtained by Monte Carlo simulation

Some conclusions can be taken upon the analysis of these results:

- Configurations that achieve the overall minimum errors tend to integrate the LOS hydrophones that attain the larger baseline between them;

- Transmitter positions that return a higher number of LOS hydrophones, have more possible configurations to choose from and therefore can be more optimized, presenting the lowest errors;

- The points directly behind the AUV that cover positions with y and z in the range [-w,w], are not contained in any line of sight region;

- When the transmitter positions have $x \leq 0$, they are in line of sight of less hydrophones than for $x > 0$, so there are fewer possible configurations and the returned best option for the various parameters are more consistent. Consequently, the returned minimum errors are usually higher than for $x > 0$;

- Transmitter positions that are located near the y-axis, almost in parallel with the circle of hydrophones, are usually covered by only four LOS regions, which correspond to the sensors that are directly closer to the target;

- For elevation angles close to $90°$ and $-90°$, the azimuth deviation is much larger than at any other position as expected, since in that region the azimuth angle is more influenced by the injected errors leading to increased deviations.

5.2.0.1 Evaluation of the line of sight regions

Upon inspecting the overall obtained results and the whole function of the system, a particular analysis is conducted to the mechanism that defines the hydrophones' LOS regions. Therefore, after evaluating the position $s(10, 10, 10)$ that is expected to have an intermediate amount of hydrophones, two additional positions are tested.

The first position to be tested is $s(-10, -10, -10)$ which inherently has less hydrophones with line of sight, due to the method's limitation for $x \leq 0$. Additionally, since it is located in the seventh octant it is expected to be only in LOS with exactly three hydrophones, thus having only one available configuration with line of sight. After simulating, figure 5.7 is obtained which verifies the concepts described. The only configuration with line of sight is number 30, composed by r_1, r_3, r_5 and r_9.

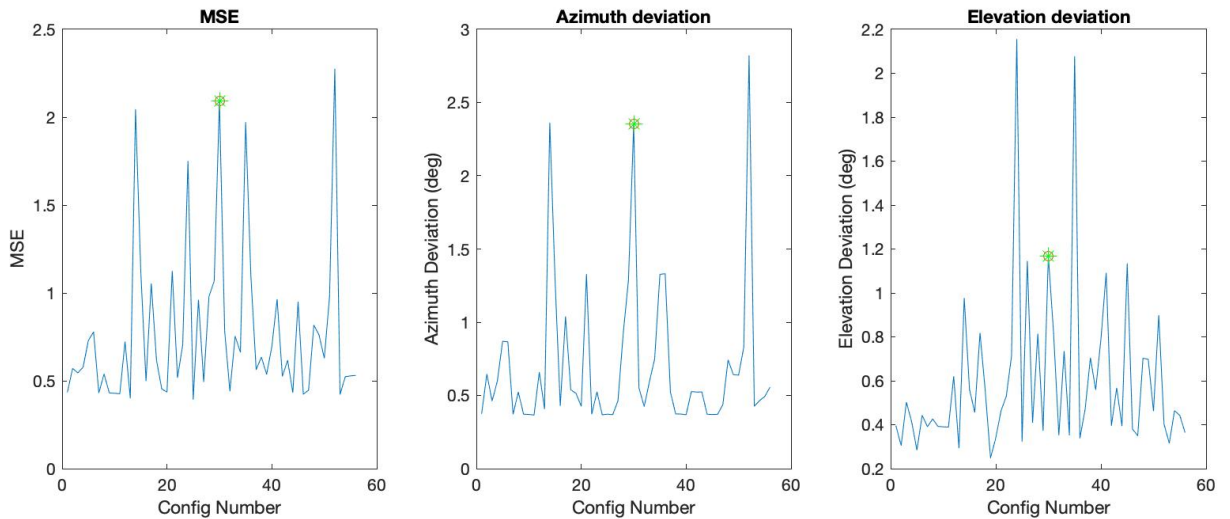Figure 5.7: Errors obtained for all configurations when estimating
position $s_{cart}(-10, -10, -10)$

Then, position $s(100, 0, 0)$ is tested. Due to its long range location and the fact that it is assumed a conic shape at the front of the vehicle, it is expected that this point has line of sight for every employed hydrophone. Figure 5.8 illustrates the simulated results which prove the theoretical expectation.
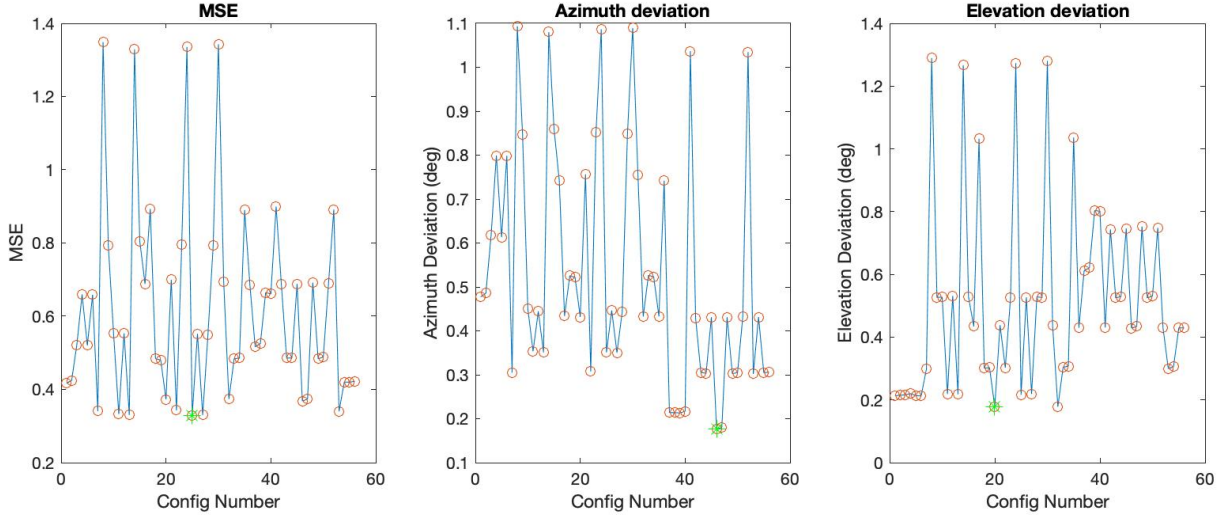
Figure 5.8: Errors obtained for all configurations when estimating
position (100,0,0)

Lastly, an extensive verification process was held in order to ensure that the returned LOS hydrophones were plausible for many other positions. Table 5.3 summarizes this search, containing a total of eleven positions spread over each octant and the reference axis. By consulting the hydrophone map illustrated in 5.1, it is possible to confirm that for every selected position the returned hydrophones are the logically expected.

	s_x	s_y	s_z	Hydrophones with LOS
x-axis	100	0	0	2, 3, 4, 5, 6, 7, 8, 9
y-axis	0	100	0	4, 6, 7
z-axis	0	0	100	2, 6, 8
1st octant	10	10	10	2, 4, 6, 7, 8
2nd octant	5	5	-1	2, 3, 4, 6, 7
3rd octant	1	-1	0	2, 3, 5, 8, 9
4th octant	1	-10	-10	3, 5, 7, 8, 9
5th octant	-100	10	10	2, 4, 6
6th octant	-1	10	-5	3, 4, 6, 7
7th octant	-1	-1	1	2, 5, 8
8th octant	-1	-100	-10	3, 5, 8, 9

Table 5.3: Hydrophones with line of sight for several *s* positions

5.2.1 Comparison with Crámer-Rao lower bound

Although the Monte Carlo approach and the Crámer-Rao bound method use distinct decision metrics, it is still worth to understand the practical differences between the implementations regarding the developed dynamic reconfigurable method.

A simulation was performed in which position $s_{cart}(0, 1000, 0)$ is estimated by both methods, obtaining the estimate cloud by the Monte Carlo approach and the uncertainty axis in Crámer-Rao bound. Figure 5.9 illustrates both data overlaid, using configuration C.
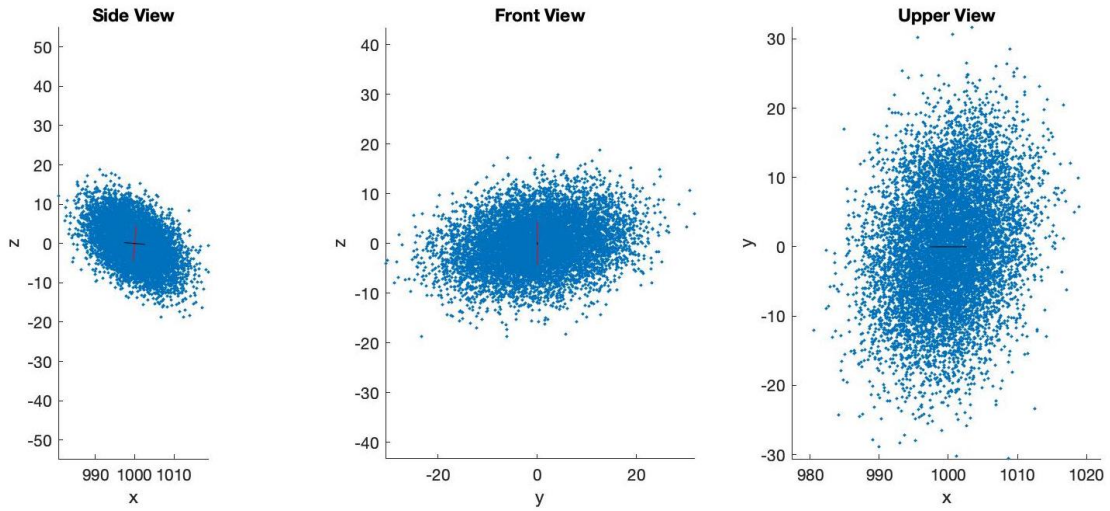

Figure 5.9: Errors obtained for all configurations when estimating
position (100,0,0)

The plot reveals that the results are clearly not coherent, which is justified by the fact that the Crámer-Rao bound assumes any linear and unbiased estimator for the configuration's evaluation, while the Monte Carlo method is a non-linear estimator, due to the least squares equation that leads to the estimation in 4.2.2.

Therefore, to avoid lack of generalization, once more it is considered that the preferable mechanism to be used for analyzing the estimation accuracy is the FIM along with the desired optimality criteria.

5.3 Optimal solution based on range

After having a comprehensive understanding on the system that is capable of determining which is the best configuration of hydrophones to estimate a specific transmitter position, an alternate scenario can be explored. We now consider that the USBL system does not reconfigure which sensor configuration it should use in order to optimize the estimation in real time. Instead, a performance study is conducted beforehand so that only two configurations are chosen to be deployed, corresponding to the ones which return the average best estimation of short and long range positions. This way, it would be possible to alternate which configuration is used

depending solely on the distance to the target. Alternatively, it is also possible to define just one overall best configuration, in cases where there is the necessity of reducing the number of deployed hydrophones or if the two obtained configurations do not have a significant difference in performance.

In the development of this mechanism, there are some adjustments and similarities from the conditions established for the previous system. Firstly, it is assumed that the hydrophones are implemented in a structure shaped like an AUV with no physical form, thus all hydrophone positions have line of sight to any point in space. Additionally, the possibilities for the hydrophone locations are increased for a more extensive study. Once again, hydrophone r_1 is integrated in all configurations and a total of 24 possibilities are considered for the remnant three. These include the same 8 positions r_2 to r_9, established for the initial setup, to which are added positions r_{10} to r_{25} defined in table 5.4. This addition corresponds to two replicated circles from the initial one, that assume the same y and z coordinates but are deviated from each other a d_x equal to 20 centimeters. Figure 5.10 illustrates all the considered possible positions for the hydrophone's deployment. Accordingly, the number of possibilities is not correspondent to combinations of three out of 24, $C(24,3)$, since these contain linearly dependent configurations, which correspond to hydrophones' positions that only differ in the x coordinate. Therefore, the total number of available combinations is 1512.

	r_{10}	r_{11}	r_{12}	r_{13}	r_{14}	r_{15}	r_{16}	r_{17}	r_{18}	r_{19}	r_{20}	r_{21}	r_{22}	r_{23}	r_{24}	r_{25}
x	0	0	0	0	0	0	0	0	d_x	d_x	d_x	d_x	d_x	d_x	d_x	d_x
y	0	0	w	-w	e	e	-e	-e	0	0	w	-w	e	e	-e	-e
z	w	-w	0	0	e	-e	e	-e	w	-w	0	0	e	-e	e	-e

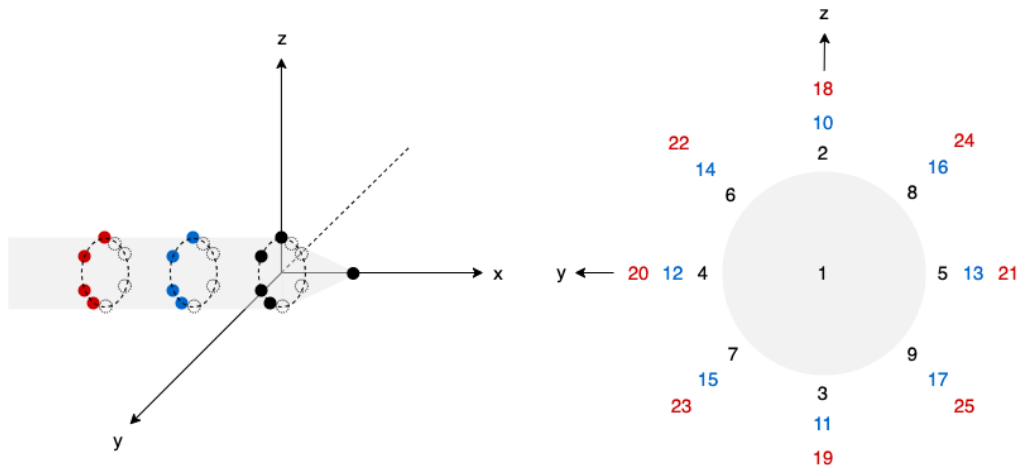Table 5.4: Additional coordinates for an implementation with 25 hydrophones

Figure 5.10: Hydrophone possible positions for optimality study based
on range

The applied algorithm is similar to the previously explained algorithms 1 and 2, with the following variations:

1. Similarly to the condition described in 4.2.5, the acoustic source positions, *s*, to be estimated are defined in spherical coordinates, where for each defined norm, the elevation component covers the interval [-90° to 90°] in steps of one and, for each elevation value, the azimuth component covers the interval [-180°, 180°] in steps of one, forming partial spheres around the reference axis' origin. The norm covers a range between 1 and 10000 meters.

2. An additional logical loop is added in algorithm 1 between lines 1 and 2, so that for each possible configuration all *s* are estimated a number of $i = 1000$ iterations.

3. the *line_of_sight* function is no longer used, as it is considered that all hydrophones have line of sight to every position *s*.

From here it is possible to analyze which are the best returned configurations, according to the chosen parameters MSE, azimuth deviation, elevation deviation and combined azimuth and elevation deviations. According to the numeric errors that are obtained, it is then possible to decide whether there is a single configuration that has evidently a better performance than the others or if there is a pair of configurations that can be used to obtain individually better estimations for short and long range.

5.3.1   Simulation results

The previously defined method was tested through a series of simulations, in which all 1512 defined configurations repeatedly estimate all positions that compose spheres of defined norms. Then, the configurations that reveals lower estimation errors are selected as the most accurate in terms of azimuth angle, elevation angle, both angles simultaneously or MSE.

The overall results do not demonstrate a specific configuration to be the clear best in short or long range for the chosen parameters. In order to associate the obtained configuration numbers to the actual hydrophone placement, figure 5.11 gathers the most relevant representations for the simulations based on range.

For performance based on azimuth, configuration number 792 shows best results for norms between 1 and 10 meters. However, for longer range the results do not tends to a specific configuration, alternating between three options.

Regarding performance based on elevation, configuration 220 is indicated for 1 to 3 meters, while for ranges going from 10 to 10000 meters, configuration 260 is the clear preferred. As can be observed in the illustration, these are structurally similar.

When evaluating azimuth and elevation accuracy simultaneously or MSE, the results are not clear and many configurations are alternated, where number 827 is the most frequent.

Additionally, it should be noted that throughout all simulated norms, for each evaluated metrics the worse performance for every position corresponded to the same configurations.

Norm	Azimuth		Elevation		Azimuth+Elevation		MSE	
	Config	Min	Config	Min	Config	Min	Config	Min
1	792	0.4730	220	0.1758	862	0.3554	862	0.4654
2	792	0.4771	220	0.1738	827	0.3905	827	0.4549
3	792	0.4820	220	0.1752	827	0.3921	860	0.4571
10	792	0.4796	260	0.1702	827	0.3918	827	0.4572
20	827	0.4893	260	0.1702	827	0.3905	827	0.4537
50	792	0.4940	220	0.1705	860	0.3947	860	0.4615
100	860	0.4881	260	0.1707	827	0.3913	860	0.4538
200	827	0.4853	260	0.1706	827	0.3889	827	0.4511
500	792	0.4886	260	0.1722	929	0.3935	862	0.4606
1000	827	0.4846	260	0.1709	827	0.3899	827	0.4524
10000	792	0.4810	260	0.1724	862	0.3920	827	0.4554

Table 5.5: Results of Monte Carlo simulation for range based estimation

To conclude, the obtained data do not show a clear tendency of two specific configurations being overall best for short and long range. This can be a result of the Monte Carlo simulation nature which originates results that do not have a clear sequence as expected. Therefore, this same experiment is repeated in the next subsection using the Fisher Information Matrix integrated in the Crámer-Rao bound method.

5.3.2   FIM simulation

Since the Fisher Information Matrix is a reliable and well know tool for evaluating a configuration's performance, then a simulation was executed for determining the best configuration for short and long range estimations. Therefore, the method was integrated in a Monte Carlo approach that tests all 1512 configurations defined previously described in this section, which integrate a total of 25 different hydrophones. For each configuration, all s positions that make up a sphere with a defined norm are used to calculate the FIM and evaluate the desired criteria. Among all, the configurations that demonstrate the preferred results correspond to the best performance in each specific criteria.

Table 5.6 summarizes the obtained results for a norm range between 1 and 10000 meters. A standard metric and three optimality criteria were observed and for each of them, the table indicates the configuration number that proved to have the best performance and the respective achieved values:

- In E-optimality, the Eigenvalue column contains the minimum larger eigenvalue found among all configurations
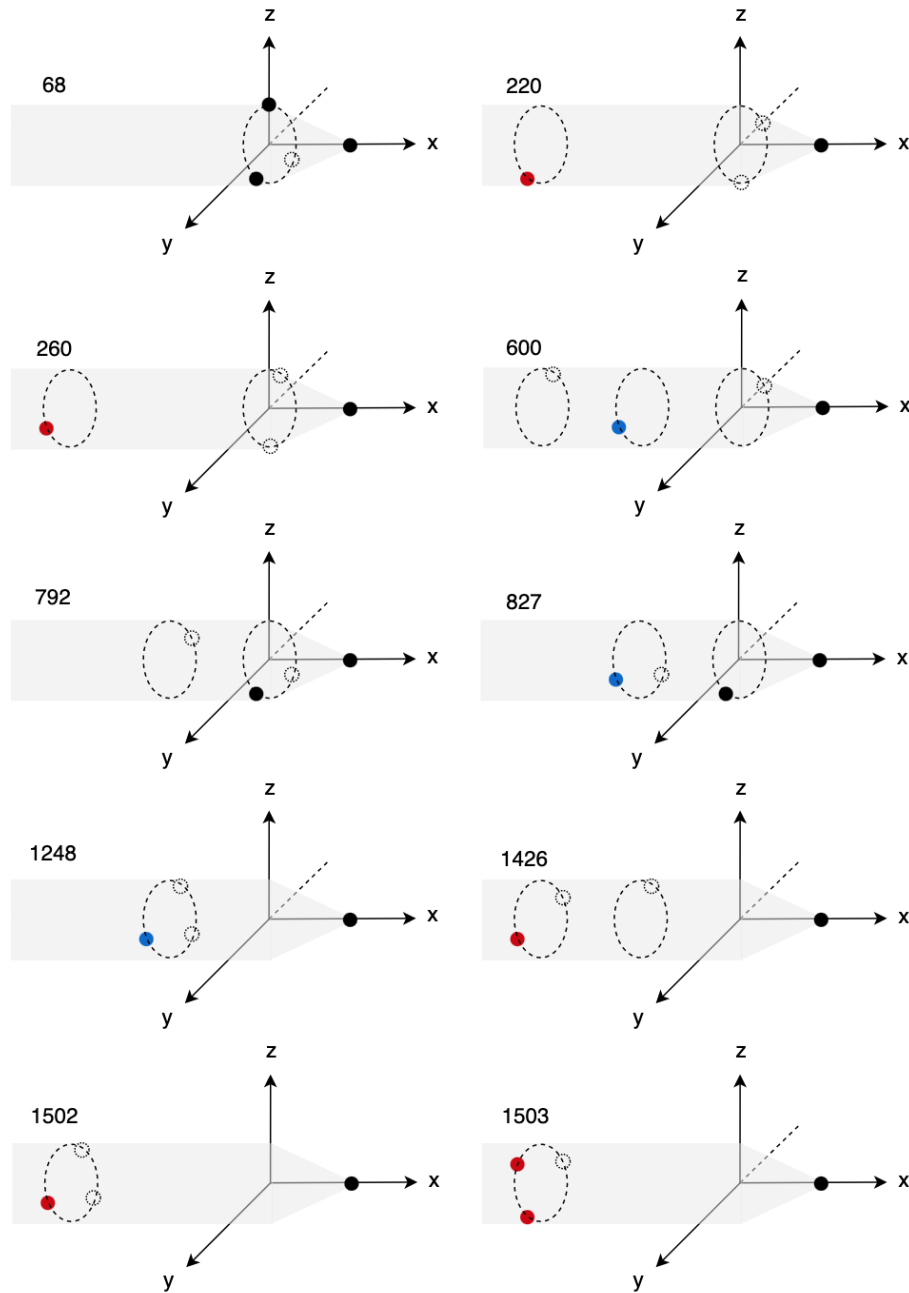
Figure 5.11: Illustration of relevant hydrophone configurations for
range based estimation

- In D-optimality, the Determinant column includes the minimum computed determinant of the inverse of the FIM for all configurations

- In A-optimality, the Trace column comprises the minimum sum of eigenvalues of the FIM among all configurations

The overall results do not demonstrate a specific configuration to be the clear best in short or long range for the chosen parameters. In order to associate the obtained configuration numbers

Norm	E-optimality		D-Optimality		A-Optimality	
	Config	Eigenvalue	Config	Determinant	Config	Trace
1	1248	$6.2{\times}10^{-3}$	1503	$1.6{\times}10^{-3}$	600	$2.3{\times}10^{-5}$
2	1248	0.012	1503	$2.5{\times}10^{-3}$	1426	$9.2{\times}10^{-5}$
3	1248	0.018	1503	$3.3{\times}10^{-3}$	1426	$2.1{\times}10^{-4}$
10	1502	0.061	1503	$7.4{\times}10^{-3}$	1426	$2.4{\times}10^{-3}$
20	1502	0.121	1503	0.012	1426	$9.6{\times}10^{-3}$
50	1502	0.303	1503	0.022	1426	0.061
100	1502	0.061	1503	0.034	1426	0.242
200	1502	1.212	1503	0.054	1426	0.968
500	1502	3.029	1503	0.100	1426	6.055
1000	1502	6.059	1503	0.159	1426	24.226
10000	1502	60.587	1503	0.737	1426	$2.42{\times}10^3$

Table 5.6: Results of FIM simulation for range based estimation

to the actual hydrophone placement, figure 5.11 gathers the most relevant representations for the simulations based on range.

By inspection, it is possible to understand that for each criterion there is a clear best configuration for short and long range. The hydrophone placement of the mentioned configuration numbers are illustrated in figure 5.11 for a more practical interpretation.

Therefore, in terms of E-optimality configuration, an approximately constant error of 0.6% is visible, where number 1248 shows the best performance for range between 1 and 3 meters, while from 10 to 10000 meters configuration 1502 is considered the best.

For D-optimality, a single configuration, number 1503, was considered the best for all defined ranges, which corresponds to an hydrophone placement that maximizes the baseline between the fixed sensor and the other three.

Finally, in terms of A-optimality configuration number 600 is indicated for norm equal to 1 meters and, for the remaining ranges, number 1426 is chosen as the preferable option.

5.4   Summary and Discussion

This chapter focuses on presenting the formulated adaptive configuration selection method, whose goal is to establish the sensor configuration that leads to the best estimation precision for a specific target position. After analyzing the results, it has proven to provide improved estimation accuracy by selecting the configuration with line of sight to the target that achieves the lower estimation error.

This mechanism could be applied to a data muling scenario, as established in chapter 1. If a discrete set of hydrophones are deployed in an mule AUV, then it is possible to adapt the selected configuration depending on the perceived angle of arrival in real-time. This allows to always use the configuration that leads to the lower estimation error and thus improve the localization accuracy.

An alternative to this method is also explored, whose goal is to select the sensor configuration that achieves the average best estimation for any target position along a sphere of defined norm. This allows to define optimal configurations based on the range, as demonstrated through simulations. As observed previously, the results of the Crámer-Rao lower bound demonstrate clear optimal configurations for both short and long range.

In practical terms, this would be useful if a maximum of two possible configurations were allowed to be deployed in an AUV, contrarily to the initial method. Considering the E-optimality as the most relevant criterion for this application, we can conclude that for short range configuration number 1248 would be optimal, whereas for long range number 1502 would be preferred.

Chapter 6

Conclusions

6.1 Summary

As stated at the beginning, the overall aim of this research work was to develop a USBL system with characteristics that lead to an improvement on localization precision, both for short and long range.

Firstly, it is presented the implementation of an hardware module that computes with precision the time differences of arrival of acoustic signals received by a set of four hydrophones. The architecture demonstrated a significant decrease of the used resources comparatively to the previous implementation and a precise calculation of the time differences of arrival. After initial field tests, a rough estimation of the obtained precision leads to conclude that the ToA measurement was improved by using the phase differences along with the correlation.

Secondly, an adaptive configuration selection method was developed which is capable of determining the optimal configuration from a discrete set of fixed hydrophones, leading to higher localization precision, i.e. lower estimation error. It uses a Monte Carlo approach for a systematic comparison between a high number of configurations and to obtain averaged estimations for more coherent results. Additionally, as an effort to improve the USBL system's viewing angle, it was integrated a mechanism that assures the continuous selection of hydrophone sets that have line of sight to the transmitter positions. The simulated results show that the method as proven to be successful, since the selected configurations always correspond to the layout that leads to the lower estimation error.

Additionally, as initially intended, the method was adjusted so that it was possible to conduct a comprehensive study on the configurations that demonstrated to be optimal for short and long range. It was concluded that using the FIM together with the preferred optimality criterion for this application, originated the most coherent results and allowed to elect the configurations that lead to an average higher precision.

This evaluation tool can be applied to any method that is capable of defining performance metrics for the evaluation of a sensor configuration. In the present research work three options were investigated, consisting on an estimator based on the TDoA measurement, an estimator that

assumes a plane wavefront and the Crámer-Rao lower bound that uses the Fisher Information Matrix. From these three options, it was concluded that the most reliable would be the third due to the independence on the chosen estimator and its wide use on literature.

6.2   Contributions

The main contributions of this dissertation are:

- A HDL system design with strict area constraints that receives signals from four different sensors and calculates the phase differences between them;

- A comparative study on three methods that evaluate the performance of sensor configurations based on several different optimality criteria;

- The adaptive configuration selection method which is capable of determining the optimal sensor configuration, from a discrete set of hydrophones in fixed positions, that leads to highest localization precision, i.e. lowest estimation error.

6.3   Future Work

The developed work arose various innovative ideas and topics according to the state of the art on localization optimization methods. Therefore, there is the intent to produce a a scientific article on the subject to be submitted in the OCEANS Conference 2021.

The adopted optimization techniques in the present work are the starting point of a topic which is not very explored in the current literature. Consequently, there are several areas that can be improved as follows:

- Implementing the developed algorithm for AoA estimation as a real-time system which can be used for decision making during underwater navigation;

- Using Machine Learning techniques in order to find the optimal hydrophone array configuration, to be positioned in an underwater vehicle;

- Integrating the estimator with a Kalman Filter or a Particle Swarm Optimization approach;

- Perform field experiments in order to examine if it is advantageous to select only the hydrophones with line of sight or if the errors obtained from propagation in the surface of the AUV are negligible;

Appendix A

Complementary Information

A.1 Hydrophone configurations numeration

In table A.1 it is possible to consult the composition of the configurations which are mentioned throughout the document. It includes the configuration number and the respective integrated hydrophones.

Table A.1: Configurations for the Monte Carlo approach with 9 employed hydrophones

Configuration number	Hydrophones			
1	1	2	3	4
2	1	2	3	5
3	1	2	3	6
4	1	2	3	7
5	1	2	3	8
6	1	2	3	9
7	1	2	4	5
8	1	2	4	6
9	1	2	4	7
10	1	2	4	8
11	1	2	4	9
12	1	2	5	6
13	1	2	5	7
14	1	2	5	8
15	1	2	5	9

Table A.1

Configuration number	Hydrophones			
16	1	2	6	7
17	1	2	6	8
18	1	2	6	9
19	1	2	7	8
20	1	2	7	9
21	1	2	8	9
22	1	3	4	5
23	1	3	4	6
24	1	3	4	7
25	1	3	4	8
26	1	3	4	9
27	1	3	5	6
28	1	3	5	7
29	1	3	5	8
30	1	3	5	9
31	1	3	6	7
32	1	3	6	8
33	1	3	6	9
34	1	3	7	8
35	1	3	7	9
36	1	3	8	9
37	1	4	5	6
38	1	4	5	7
39	1	4	5	8
40	1	4	5	9
41	1	4	6	7
42	1	4	6	8
43	1	4	6	9

Table A.1

Configuration number	Hydrophones			
44	1	4	7	8
45	1	4	7	9
46	1	4	8	9
47	1	5	6	7
48	1	5	6	8
49	1	5	6	9
50	1	5	7	8
51	1	5	7	9
52	1	5	8	9
53	1	6	7	8
54	1	6	7	9
55	1	6	8	9
56	1	7	8	9

References

[1] J. Liang, "Fifteen percent of ocean floor now mapped," Jun 2019. [Online] Available: https://www.deeperblue.com/fifteen-percent-of-ocean-floor-now-mapped/. [Accessed Oct. 28, 2019].

[2] H. P. Tan, R. Diamant, W. K. G. Seah, and M. Waldmeyer, "A survey of techniques and challenges in underwater localization," *Ocean Engineering*, vol. 38, no. 1, pp. 1663–1676, 2011.

[3] F. B. Jensen, W. A. Kuperman, M. B. Porter, and H. Schmidt, "Fundamentals of Ocean Acoustics," in *Computational Ocean Acoustics*, pp. 3–17, Springer Science & Business Media, second ed., 2011.

[4] M. C. Domingo, "Overview of channel models for underwater wireless communication networks," *Physical Communication*, vol. 1, no. 3, pp. 163–182, 2008.

[5] M. Stojanovic and J. Preisig, "Underwater Acoustic Communication Channels: Propagation Models and Statistical Characterization," *IEEE Communications Magazine*, vol. 47, no. 1, pp. 84–89, 2009.

[6] J. M. F. M. aes, "Improving Time of Arrival Estimation Using Encoded Acoustic Signals," Master's thesis, Faculty of Engineering of the University of Porto, Porto, jul 2018.

[7] D. E. Chaitanya, C. V. Sridevi, and G. S. B. Rao, "Path loss analysis of Underwater communication systems," in *IEEE Technology Students' Symposium*, pp. 65–70, IEEE, 2011.

[8] S. Gezici, "A survey on wireless position estimation," *Wireless Personal Communications*, vol. 44, no. 3, p. 263–282, 2008. Springer Science & Business Media.

[9] B. M. R. Bharathi and A. R. Mohanty, "Underwater Sound Source Localization by EMD-Based Maximum Likelihood Method," *Acoustics Australia*, vol. 46, no. 2, pp. 193–203, 2018.

[10] V. Chandrasekhar, W. K. Seah, Y. S. Choo, and H. V. Ee, "Localization in underwater sensor networks: survey and challenges," in *WUWNet '06: Proceedings of the 1st ACM international workshop on Underwater networks*, pp. 33–40, 2006.

[11] J. Esteves, A. Carvalho, and C. Couto, "Generalized geometric triangulation algorithm for mobile robot absolute self-localization," in *2003 IEEE International Symposium on Industrial Electronics*, vol. 1, (Rio de Janeiro, Brazil), pp. 346–351, 2003.

[12] A. P. Pandian, T. Senjyu, S. M. S. Islam, and H. Wang, "Weighted Trilateratiton and Centroid Combined Indoor Localization in Wifi Based Sensor Network," in *Proceeding of the International Conference on Computer Networks, Big Data and IoT (ICCBI - 2018)*, pp. 163–166, jul 2019.

[13] M. Erol-Kantarci, H. T. Mouftah, and S. Oktug, "A Survey of Architectures and Localization Techniques for Underwater Acoustic Sensor Networks," *IEEE Communications Surveys & Tutorials*, vol. 13, no. 3, pp. 487–502, 2011.

[14] X. You, Y. Wu, M. Zhu, X. Li, and L. Zhang, "Low Complexity Short Baseline Localization Algorithm Based on Taylor Expansion," in *2019 IEEE International Conference on Signal Processing, Communications and Computing*, pp. 1–5, IEEE, 2019.

[15] K. G. Kebkala and A. I. Mashoshinc., "AUV Acoustic Positioning Methods," *Gyroscopy and Navigation*, vol. 8, pp. 80–89, sep 2017.

[16] D. Sun, J. Ding, C. Zheng, and W. Huang, "An Underwater Acoustic Positioning Algorithm for Compact Arrays With Arbitrary Configuration," *IEEE Journal of Selected Topics in Signal Processing*, vol. 13, pp. 120–130, mar 2019.

[17] E. GmbH, "Underwater USBL Positioning Systems," 2018. [Online] Available: https://evologics.de/usbl. [Accessed Jan. 26, 2020].

[18] E. GmbH, "S2C Technology," 2018. [Online]. Available: https://evologics.de/s2c-technology [Accessed Jan. 26, 2020].

[19] E. GmbH, "18/34 communication and positioning devices," 2018. [Online]. Available: https://evologics.de/acoustic-modem/18-34 [Accessed Jan. 26, 2020].

[20] E. GmbH, "S2C R 12/24 USBL communication and positioning device," 2018. [Online]. Available: https://evologics.de/acoustic-modem/12-24/usbl-serie [Accessed Jan. 26, 2020].

[21] Sonardyne, "MICRO-RANGER 2 SHALLOW WATER USBL SYSTEM," 2020. [Online]. Available: https://www.sonardyne.com/product/micro-ranger-2-shallow-water-usbl-system/ [Accessed Feb. 3, 2020].

[22] K. Maritime, "HiPAP - HIGH PRECISION ACOUSTIC POSITIONING," 2016. [Online]. Available: https://www.kongsberg.com/maritime/products/Acoustics-Positioning-and-Communication/acoustic-positioning-systems/hipap-models/ [Accessed May 2, 2020].

[23] A. N. Bishop, B. Fidan, B. D. O. Anderson, K. Doğançay, and P. N. Pathirana, "Optimality analysis of sensor-target localization geometries," *Automatica*, vol. 46, no. 3, pp. 479–492, 2010.

[24] E. Rady, M. M. E. A. El-Monsef, and M. M. Seyam, "Relationships among several optimality criteria," *Interstat*, vol. 15, no. 6, pp. 1–11, 2009.

[25] C. Tholen, T. A. El-Mihoub, L. Nolle, O. Ralle, and R. Rofallski, "Optimal receiver configuration of short-baseline localisation systems using particle swarm optimisation.," in *ECMS*, pp. 25–31, 2020.

[26] A. M. Bonito, "Acoustic system for ground truth underwater positioning in DEEC's test tank," Master's thesis, Faculty of Engineering of the University of Porto, Porto, jul 2019.

[27] J. Valls, T. Sansaloni, A. Perez-Pascual, V. Torres, and V. Almenar, "The use of cordic in software defined radios: A tutorial," *IEEE Communications Magazine*, vol. 44, no. 9, pp. 46–50, 2006.

[28] A. A. Assef, B. M. Ferreira, J. M. Maia, and E. T. Costa, "Modeling and fpga-based implementation of an efficient and simple envelope detector using a hilbert transform fir filter for ultrasound imaging applications," *Research on Biomedical Engineering*, vol. 34, no. 1, pp. 87–92, 2018.

[29] J. Reis, M. Morgado, P. Batista, P. Oliveira, and C. Silvestre, "Design and experimental validation of a usbl underwater acoustic positioning system," *Sensors*, vol. 16, no. 9, p. 1491, 2016.

[30] B. Ferreira, A. Matos, and N. Cruz, "Optimal positioning of autonomous marine vehicles for underwater acoustic source localization using TOA measurements," in *2013 IEEE International Underwater Technology Symposium (UT)*, pp. 1–7, IEEE, 2013.